

New Strategy for the Conformational Analysis of Carbohydrates Based on NOE and ^{13}C NMR Coupling Constants. Application to the Flexible Polysaccharide of *Streptococcus mitis* J22[†]

Manuel Martin-Pastor and C. Allen Bush*

Department of Chemistry and Biochemistry, University of Maryland-Baltimore County, Baltimore, Maryland 21250

Received February 22, 1999; Revised Manuscript Received April 19, 1999

ABSTRACT: For complex oligosaccharides, which are relatively rigid with modest excursions from a single minimum energy conformation, it is straightforward to build conformational models from NOE data. Other oligosaccharides are more flexible with transitions between distinct minima separated by substantial energy barriers. We show that modeling based on scalar coupling data is superior to NOE-based modeling for the latter case. Long range ^{13}C – ^{13}C and ^{13}C – ^1H coupling constants measured for the heptasaccharide repeating subunit of the cell wall polysaccharide from *Streptococcus mitis* J22 are correlated with individual glycosidic dihedral angles, effectively uncoupling the degrees of freedom of the oligosaccharide and allowing a search for combinations of dihedral angles which are energetically reasonable, i.e., with no bad van der Waals contacts, and which can be combined to satisfy all the measured J values. Allowed values of the individual angles can then be combined to search for overall oligosaccharide conformations which contribute to the ensemble. We show that while the polysaccharide from *S. mitis* J22 is flexible, requiring multiple conformations, most of the flexibility is localized to a few bonds and only a rather small number of conformations is required to reproduce the experimental NOE and scalar coupling data.

A central question in the conformation and dynamics of complex oligosaccharides and polysaccharides is whether a given structure is “flexible” (1–3). In fact, no oligosaccharide is likely to be truly rigid since puckering of the pyranoside ring and fluctuations of the glycosidic dihedral angles must occur to some extent in all cases. But the currently available data allows for classification of the types of internal motion in oligosaccharides into two distinct types. We will identify internal motion of the first kind as rapid motion on a picosecond time scale of the internal degrees of freedom within a local minimum with limited excursions of the dihedral angles. Oligosaccharides exhibiting this type of internal motion are sometimes called “rigid” in the sense that experimental NOE¹ data may agree with that calculated for a model having a single conformation. The blood group oligosaccharides, especially the Lewis type, are probably the best example of a relatively rigid conformation exhibiting primarily internal motion of the first kind (4–9).

In addition to this first kind of motion, more flexible oligosaccharides can also present a second kind of internal motion which is characterized by larger excursions of glycosidic dihedral angles crossing high-energy barriers from one well-defined minimum to another. The existence of this second kind of flexibility may be inferred when the experimental data are not compatible with a single confor-

mation. The time scale of such motions depends on the height of the barrier separating the energy minima and could range from nanoseconds to microseconds. At this point, we have available limited information, either experimental or theoretical, regarding the kinetics of such conformational transitions.

It is straightforward to construct a credible model for the Lewis oligosaccharides, and the results of most published studies are in general agreement for these systems. The results of computer molecular modeling depend strongly on neither the modeling methodology used nor on the technique for treatment of the solvent. On the other hand, studies of a number of oligosaccharides have appeared in the literature for which the experimental NOE data do not agree with a single conformational model (10).

For the mannose-containing oligosaccharides of the N-linked glycopeptides, data indicate extensive internal motion of the second kind and building of detailed models has been difficult and somewhat controversial (3, 11, 12). The virtual conformation model considers exchange among a number of low-energy conformers and requires accurate statistical weights for each important conformer as well as information about the kinetics of the conformational exchange (13). It has proven to be difficult to extract all this information from experimental NOE data, and computer molecular modeling of large complex oligosaccharides has also encountered some obstacles. Explicit treatment of solvent water appears to be required for molecular dynamics simulations of sugars and while good agreement between solvent simulations and the available experimental data is found for simple disaccharides (10, 14), simulations of larger branched structures have been less successful.

[†] Research supported by NSF Grant MCB9724133.

* To whom correspondence should be addressed.

¹ Abbreviations: NOE, nuclear Overhauser effect; HMQC-NOESY, heteronuclear multiple quantum coherence–nuclear Overhauser effect spectroscopy; SA, simulated annealing; r-SA, restrained simulated annealing; SVD, singular value decomposition.

Table 1: Experimental and Calculated H–C and C–C Coupling Constants for the Different Glycosidic Linkages of the Polysaccharide of *S. mitis* J22 Using the Three Main Conformers of Solution 1

linkage		ϕ				ψ		
		$^3J_{\text{H1C1O1Cx}}$	$^3J_{\text{C2C1O1Cx}}$	$^2J_{\text{C1O1Cx}}$	$\langle\phi\rangle$ (deg) ^d	$^3J_{\text{HxCxO1C1}}$	$^3J_{\text{Cx-1CxO1C1}}$	$^3J_{\text{Cx+1CxO1C1}}$
AB	solution 1	1.4	<i>c</i>		−63	1.7	0.9	3.6
	exp	1.5	1.7	−1.8	−50	1.5	<0.8	2.5
BC	Solution 1	1.9	2.5		−62	2.1	0.8	<i>c</i>
	exp	2.0	2.3	−1.8	−50	2.1	<0.8	2.0
GB	solution 1	1.0	3.5		69	3.5	3.2	0.2
	exp	1.5	ol ^e	−2.3	70	4.1	ol	<0.8
CD	solution 1	2.1	1.0		29	2.6 ^a	2.0	
	exp	1.5	<0.8	−1.4	35	1.9	2.2	
DE	solution 1	1.7	2.6		37	2.0 ^b	2.5	
	exp	1.5	2.6	−1.7	50	1.3	2.5	
EF	solution 1	2.8	3.4		46	1.9	3.6	0.8
	exp	2.4	ol	−2.0	60	1.3		<0.8

^a Calculated for H6dproS. ^b Calculated for H6eproR. ^c This coupling constant is affected by in plane oxygen and eq 3 is not applicable. ^d Average ϕ dihedral angle calculated for the set of conformations or experimentally estimated from $^2J_{\text{coc}}$ using the projection sum rule. ^e ol, overlapping signal.

The hydroxymethyl dihedral angle is defined as ω , O6–C6–C5–O5. The pucker of the galactofuranose residue **d** is described by a single variable called the phase angle, P (eq 1) (30):

$$\tan(P) = \frac{(\nu_4 + \nu_1) + (\nu_3 + \nu_0)}{2\nu_2[\sin(36) + \sin(72)]} \quad (1)$$

In this equation, ν_0 is defined by the four atoms C4–O4–C1–C2, ν_1 is defined by O4–C1–C2–C3, ν_2 is defined by C1–C2–C3–C4, ν_3 is defined by C2–C3–C4–O4, and ν_4 is defined by C3–C4–O4–C1. For the galactofuranose ring, an additional conformational dihedral angle is defined as γ C6–C5–C4–O4.

A dynamical simulated annealing calculation (SA) (31) was performed for the heptasaccharide repeating unit of polysaccharide J22 using the CVFF force field within the InsightII/Discover programs (32) of Biosym Technologies (San Diego, CA). A linear distance-dependent dielectric constant of $80r$ was used to diminish electrostatic effects. The starting structure was the global minimum reported previously (23, 27). The protocol for SA consisted of an initialization period where the system is heated to 600 K, followed by 2000 ps of molecular dynamics simulation at 600 K using a integration step of 1 fs. After simulation at 600 K for 2 ps, the system was cooled and minimized using 2000 steps of conjugate gradient. The resulting structure was stored for analysis, then reheated to 600 K and reintroduced in the SA algorithm. The minimization and dynamics steps were repeated 1000 times for a total of 2000 ps of MD.

Restrained simulated annealing simulations (r-SA) were calculated in which distance restraints were applied only for the strongest interglycosidic NOEs observed (H5a–H3b, H1a–H3b, H1a–H2b, H2b–H1g, H1a–H1g, H1b–H4c) based on the data from Table 2 of Xu and Bush (15, 27). For the glycosidic dihedral angles, ϕ/ψ , restraints were deduced from simultaneous solutions of the coupling constant equations as will be described (see Table 2). As the solutions of the interglycosidic H–C and C–C coupling constant data revealed that some glycosidic dihedral angles can adopt more than one conformation, different combinations of dihedral angle restraints were explored. A total of 64 simulations were performed using a different combination of glycosidic

dihedral angle restraints for the heptasaccharide repeating unit, while the NOE distance restraints were the same in all of them. A flat bottomed pseudoharmonic potential function was applied for the dihedral angle and distance restraints. In these simulations, no energy penalty is applied if the target dihedral angle is within $\pm 5^\circ$ over the values deduced for each dihedral angle in Table 2. This choice was observed to restrict the dihedral angle within $\pm 15^\circ$ of the target value. For the NOE restraints, no penalty is applied if the inter-proton distance is in the range 2.5–3.7 Å. For every combination, a different starting structure was built, minimized using the restraints, and then submitted to the r-SA. The total simulation time was 250 ps for each simulation. The rest of the conditions such as temperature, cooling period, etc. were the same as described for the unrestricted SA.

The analysis of the SA and r-SA trajectories was performed using the Analysis module of the InsightII program. Pyranoside chair conformations other than the normal 4C_1 and 1C_4 forms were rejected as were conformations with energy over 6 kcal mol^{−1} over the corresponding global minimum. Plots of different dihedral angles and distributions obtained for the heptasaccharide J22 were represented using the Origin program (33).

Of the 64 r-SA calculations, 20 whose energy fell within 6 kcal mol^{−1} over the global minimum were analyzed by a singular value decomposition (SVD) method (34) using the program Mathcad (35). Statistical weights were calculated to give best agreement between calculated and experimental coupling constants. For each of the resulting combinations, the global minimum structure or one within 6 kcal mol^{−1} over the global minimum was selected in order to simulate the theoretical coupling constants.

A final r-SA calculation was performed for each of the three most populated conformers found to contribute to the ensemble deduced by SVD. The NOE restrictions applied, in addition to those previously used for the strongest interglycosidic NOEs, included an additional NOE restraint (H1d–H2d) to fix the conformation of the Galf ring **d** in agreement with the experimental data. The glycosidic dihedral angle restrictions applied in each simulation were those deduced in the text for the corresponding conformation. In a simulation time of 2 ns, a total of 1000 minimized

Table 2: Relevant Solutions Obtained for the Linear Combination of Conformations in Agreement with both the Coupling Constants and the SA Distribution (Figure 3) for the Glycosidic Torsion Angles of the Polysaccharide from *S. mitis* J22

torsion	coupling constants	number of conformers					
		1		2		3	
		angle	Σp_i	angle	Σp_i	angle	Σp_i
$\phi_{H ab}$	${}^3J_{H1C1O1Cx}$ ${}^2J_{C1O1Cx}$	-60 ± 5	1.00	-70 ± 5 25 ± 5	0.80 ± 0.06 0.20 ± 0.06	same as 2	
$\psi_{H ab}$	${}^3J_{HxO1C1}$ ${}^3J_{Cx-1CxO1C1}$	-60 ± 5	1.00	-55 ± 5 -65 ± 5	0.80 ± 0.02 0.20 ± 0.02	same as 2	
$\phi_{H bc}$	${}^3J_{H1C1O1Cx}$ ${}^3J_{C2C1O1Cx}$ ${}^2J_{C1O1Cx}$	no solution		-75 ± 5 15 ± 10	0.65 ± 0.06 0.35 ± 0.06	-70 ± 5 20 ± 5 30 ± 5	0.68 ± 0.02 0.22 ± 0.02 0.10 ± 0.02
$\psi_{H bc}$	${}^3J_{HxO1C1}$ ${}^3J_{Cx-1CxO1C1}$	-55 ± 5	1.00	-55 ± 5 -40 ± 5	1.0 ± 0.15 0.0 ± 0.15	same as 2	
$\phi_{H gb}$	${}^3J_{H1C1O1Cx}$ ${}^2J_{C1O1Cx}$	no solution		70 ± 5 30 ± 10	0.90 ± 0.02 0.10 ± 0.02	same as 2	
$\psi_{H gb}$	${}^3J_{HxO1C1}$ ${}^3J_{Cx+1CxO1C1}$	no solution		multiple solutions -35 to 55		same as 2	
$\phi_{H cd}$	${}^3J_{H1C1O1Cx}$ ${}^3J_{C2C1O1Cx}$ ${}^2J_{C1O1Cx}$	no solution		-70 ± 5 120 ± 5	0.46 ± 0.02 0.54 ± 0.02	-60 ± 5 -40 ± 5 110 ± 5	0.40 ± 0.04 0.10 ± 0.04 0.50 ± 0.04
$\psi_{O cd}$	${}^3J_{HxO1C1}$ ${}^3J_{Cx-1CxO1C1}$	no solution		multiple solutions -180 to -10080 to 180		same as 2	
ϕ_{Hde}	${}^3J_{H1C1O1Cx}$ ${}^3J_{C2C1O1Cx}$ ${}^2J_{C1O1Cx}$	no solution		70 ± 5 -40 ± 5	0.76 ± 0.02 0.24 ± 0.02	same as 2	
$\psi_{O de}$	${}^3J_{HxO1C1}$ ${}^3J_{Cx-1CxO1C1}$	no solution		multiple solutions -180 to -7080 to 180		same as 2	
$\phi_{H ef}$	${}^3J_{H1C1O1Cx}$ ${}^2J_{C1O1Cx}$	50 ± 5	1.00	multiple solutions -20 to 70		same as 2	
$\psi_{H ef}$	${}^3J_{HxO1C1}$ ${}^3J_{Cx+1CxO1C1}$	-55 ± 5	1.00	-60 ± 5 -40 ± 5	0.86 ± 0.02 0.14 ± 0.02	same as 2	

structures was obtained in each of the three cases. The rest of the conditions used for the simulations such as force field, temperature, etc., were the same as previously described for r-SA. From these simulations were obtained the final structures for the three most populated conformers.

A qualitative analysis of the experimental NOE data was performed using the three most populated conformations. NOE distance contours of some interresidue distances were generated for different disaccharide components of the J22 polysaccharide by performing rigid grid-search rotation around the ϕ and ψ angles of a minimized structure for the disaccharide. The representation of the contours was made using the program Origin (33).

Coupling Constant Correlation. Vicinal C–H coupling constants were correlated with dihedral angle using the function in eq 2

$${}^3J_{COCH} = 5.7 \cos^2(\theta) - 0.6 \cos(\theta) + 0.5 \quad (2)$$

$${}^3J_{COCC} = 3.49 \cos^2(\theta) + 0.16 \quad (3)$$

proposed by Tvaroska et al. (36). Recently, Serianni and co-workers (20) have deduced a ${}^3J_{COCC}$ Karplus-type correlation curve (eq 3) based on their experimental and computational studies with a wide range of conformationally restricted carbohydrates having specific ^{13}C labels. The combined use of eqs 2 and 3 provides sufficient experimental information to deduce conformations adopted by the glycosidic linkages even for the case of flexible carbohydrates in which more than one conformation exists in solution.

An approximate correlation relating ${}^2J_{C1O1Cx}$ with the average glycosidic angle $\langle\phi_H\rangle$ was derived from the projec-

tion sum resultant method by Serianni and co-workers (21, 37, 38). First, the projection sums were calculated from the cosine dependence given by Church et al. (21) for the different glycosidic linkages which occur in the polysaccharide of Chart 1. The projection resultants were related to the coupling constants using the data of Scheme 6 in ref 21, producing the approximate correlation illustrated in Figure 1. Since the projection resultant method does not provide an exact relationship with experimental ${}^2J_{C1O1Cx}$ data, the use of these data in the modeling was less restrictive than vicinal coupling data as will be explained below.

The conformation of the furanose ring of residue d in polysaccharide *S. mitis* J22 was studied by using the structural information deduced from ${}^1J_{CH}$, ${}^3J_{COCC}$, and ${}^3J_{CCC}$ coupling constants and NOE data. These data can be related to furanoside pucker and was used to select conformations in the overall model as will be explained below.

RESULTS

The method proposed for modeling of flexible carbohydrates contains three stages, the first step of which is extensive exploration of the conformational space allowed for the heptasaccharide repeating unit of the polysaccharide using an unrestricted simulated annealing calculation (SA). A second stage is to find all the simultaneous solutions of the Karplus correlation curves in eqs 2 and 3 in agreement with experimental data. Only energetically reasonable values of the glycosidic dihedral angles deduced from the first step were included in this step. Whenever no single dihedral angle was found to agree within the experimental error, a linear combination of different angles and statistical weights was

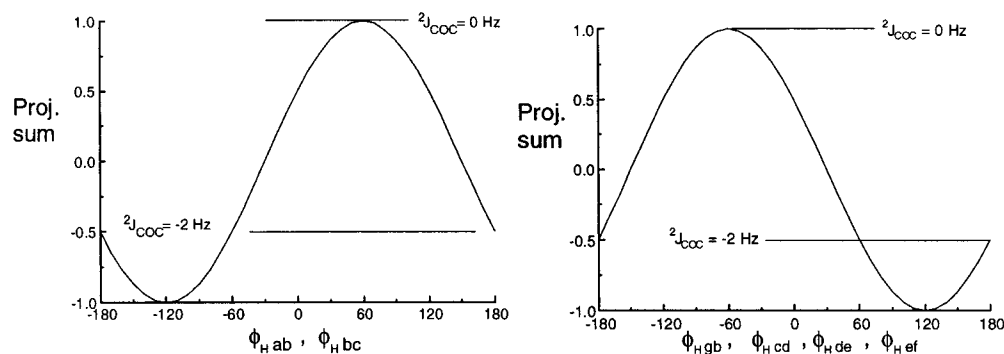


FIGURE 1: Projection resultant rule as a function of the glycosidic ϕ_H dihedral angle for the different linkages of the polysaccharide from *S. mitis* J22. Experimental ${}^2J_{C1O1C_x}$ coupling constants for resultants of -0.5 and 1.0 are indicated by a horizontal line.

proposed to explain the observed coupling constants (eq 4).

$$J_{\text{exp}} = \sum_i p_i J_i \quad (4)$$

In this equation, the coefficient p_i represents the statistical weight of conformer i in the ensemble. J_{exp} is the observed coupling constant and J_i refers to the values calculated for each single conformation using eq 2 or eq 3. In a third step, all the solutions are combined to built reasonable models using a restrained simulated annealing calculation (r-SA). Finally, the capacity of these models to reproduce all the available experimental data is tested.

Stage 1: Simulated Annealing (SA) of J22 Polysaccharide. To explore the conformational space allowed for the heptasaccharide repeating unit of J22, a simulated annealing strategy (SA) was used as described in the Materials and Methods. This stochastic method, which is commonly applied to explore conformations of molecules with many degrees of torsional freedom, has been used for oligosaccharides (39–41). It has been pointed out that when using SA calculations for carbohydrates, some of the pyranose rings may suffer transitions to distorted chair conformations, which remain during a considerable part of the trajectory diminishing the efficiency of the method. Nevertheless, in these simulations, the conditions such as temperature and time for the heating and cooling periods can be adjusted to minimize the number of those anomalous conformations resulting from inaccuracy in the force field (39–41). The SA calculations performed for the heptasaccharide repeating unit of J22 under the conditions described in the Materials and Methods resulted in a $\sim 12\%$ of these distorted ring conformations. From 1000 minimized structures, a total of 56 low-energy conformations was obtained in a range up to 6 kcal mol $^{-1}$ over the global minimum. The dihedral angles ϕ and ψ for these low-energy conformers are found in a narrow region of the conformational map for the glycosidic linkages *ab*, *bc*, *gb*, and *ef*, while for the glycosidic linkages *cd* and *de*, the minima are more spread in the map (see Figure 2 and Figure S1 of the Supporting Information). These results are not unexpected as the glycosidic linkages *cd* and *de* are of 1 \rightarrow 6 type which show a higher conformational flexibility. The hydroxymethyl torsion angles ω_a , ω_c , and ω_e of the 56 minima can adopt any of the three possible staggered conformations *gg* (-60°), *gt* (60°), and *tg* (180°). For ω_d , *gg* and *gt* conformers predominate over *tg*. γ Torsion of the galactofuranose ring *d* adopts predominantly values around 60 or -60° , and the phase parameter P of this ring adopts

nearly a continuum distribution between -60 and 60° corresponding to different north and south conformations of the ring (see Figure S2 of the Supporting Information).

Stage 2: Simultaneous Solutions to Coupling Constant Data for the Polysaccharide. Table 1 gives the experimental coupling constant values corresponding to the different glycosidic torsion angles of the polysaccharide from *S. mitis* J22. An attempt to obtain directly a value of the ϕ_H or ψ_H dihedral angle from these data using eqs 2 and 3 reveals that there is no solution within the experimental error for some of the glycosidic torsion angles, which means that the data are not compatible with a single conformation. A linear combination of different conformers is proposed to explain the observed coupling constants by using eq 4.

Application of eqs 2 and 3 to the experimental coupling constants requires converting the angles of the H–C–O–C and C–O–C–C coupling pathways, respectively, to the definition of ϕ_H and ψ_H given in the text. The conversion depends on the configuration at C-1 (α or β , D or L) and at the C-x atom (D or L). Another point to consider is that eq 3 is not applicable when oxygen atoms lie in the coupling plane, which leads to an enhancement in the experimental coupling constant that is not predicted by this equation (20). Such in-plane oxygen atoms occur for two coupling constants measured in the J22 polysaccharide. The coupling constant ${}^3J_{C1-O1-C_x-C_{x+1}}$ in the glycosidic linkage between residues *b*–*c* has O-5 of residue *b* in plane. The other case is the coupling constant ${}^3J_{C2-C1-O1-C_x}$ involving the glycosidic linkage between residues *g*–*b* for which an oxygen in plane conformation occurs for O2 of residue *g*. These two coupling constants were not used in the analysis.

The range of glycosidic dihedral angles allowed by the energy calculation was estimated from the 56 minima obtained in the SA calculation as plotted in Figure 2. Within these ranges, many conformers could be built without steric conflicts. Inaccuracies in the energy calculation and the limited time of the SA simulation require that the plot of Figure 2 not be interpreted as statistical weights for the individual conformers, but the regions of significant population can be used as a basis for deriving accurate angles and statistical weights from the experimental scalar coupling data. For a given glycosidic torsion, all the possible linear combinations of these allowed angles according to SA were combined using a simple computer program which performs a grid search of angles and statistical weights. At every point, the program evaluates the theoretical coupling constants according to eqs 2–4 and compares them with the experi-

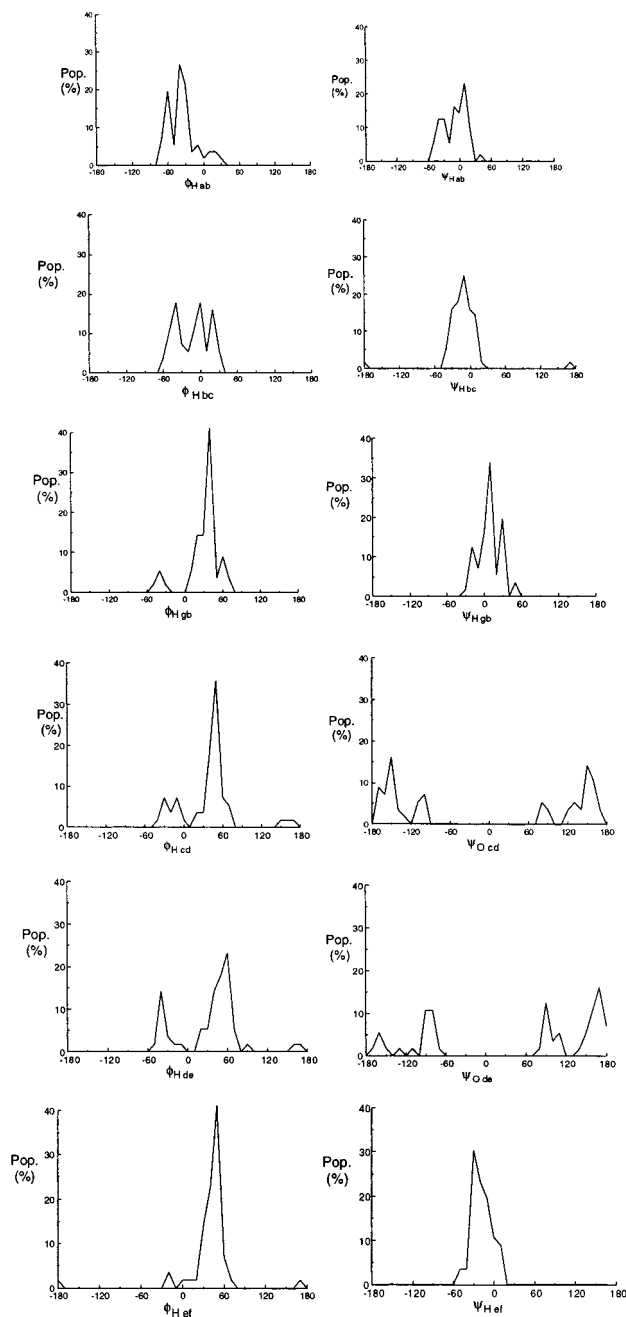


FIGURE 2: Distributions for the glycosidic torsion angles of the heptasaccharide from *S. mitis* J22 for the 56 lowest energy conformations obtained by SA.

mental ones related to that glycosidic torsion.

During the grid search, each angle was incremented in 5° steps and the statistical weights incremented in 0.02 steps. In every step, a combination is rejected if the calculated coupling constants are beyond the experimental error or if any angle differs by more than 15° from the closest populated point ($>0\%$) in the corresponding distribution of Figure 2. The number of different conformers (variable i in eq 4) used ranged from 1, which gave no solution for most of the angles, up to 5 which will be seen to be an adequate maximum to explain our data. The range of angles scanned in the grid search goes from -180 to 180° , but to reduce the computational cost, for cases when $i \geq 3$, the range was limited to the populated zones of the distribution of Figure 2. $\langle\phi_H\rangle$ for the combination was calculated and compared with that

deduced from $^2J_{C1O1C_x}$ data. The combination is rejected for discrepancies greater than 15° (Figure 1). Any conformation in the distribution with a statistical weight greater than 0.1 was stored for use in step 3 of the method.

The results of the search summarized in Table 2 show that data for some of the glycosidic torsions, such as $\phi_{H ab}$, $\psi_{H ab}$ and $\psi_{H bc}$, $\phi_{H ef}$ and $\psi_{H ef}$ can be explained by a single conformation. The rest of the torsions require a minimum of two different conformations. Nevertheless, if the number of conformations is higher than 2, no new combinations of angles and statistical weights are found for most of the glycosidic linkages. The only exceptions are $\phi_{H bc}$ and $\psi_{H cd}$ for which a slight variation of the two most populated angles occurs when using three conformers rather than 2. In all cases, it was observed that increasing the number of conformers to 4 or 5 results in no new combinations that explain the data. This fact is due to the restrictive nature of both the experimental coupling constants and the molecular modeling distribution as well as the criteria used for rejecting conformers with population lower than 0.1.

Results in Table 2 show that eight of the 12 glycosidic torsions of J22, $\phi_{H ab}$, $\psi_{H ab}$, $\phi_{H bc}$, $\psi_{H bc}$, $\phi_{H gb}$, $\phi_{H cd}$, $\phi_{O de}$, and $\psi_{H ef}$, are very restricted in terms of angles and statistical weights. For three of the remaining torsions, $\psi_{H gb}$, $\psi_{O cd}$, $\psi_{O de}$, the experimental data is not so restrictive and multiple solutions can exist within a wider range of angles and statistical weights. Two of these three torsions, $\psi_{O cd}$ and $\psi_{O de}$, are involved in (1 \rightarrow 6) type linkages where a higher flexibility could be expected. The remaining torsion $\phi_{H ef}$ is a peculiar case because the experimental couplings can be explained both using a single conformation or also with two conformers whose angles are not well-defined by the coupling constants.

Stage 3: Restrained Simulated Annealing (r-SA) of J22 Polysaccharide. Data in Table 2 were derived from consideration of individual glycosidic dihedral angles. When these are combined to produce the heptasaccharide subunit, new interresidue interactions can appear restricting the overall conformation. The influence of these interactions was incorporated through restrained simulated annealing calculations (r-SA) using restraints derived from Table 2 which lists the low-energy conformations which can be combined to give correct experimental scalar coupling constants.

While all the restraints deduced could be applied simultaneously in a unique r-SA simulation with time-averaged restraints, it is simpler to apply them in groups to improve the effectiveness exploring the conformational space available. Combinations of the restraints were selected from Table 2 for use in generating overall conformations which might contribute to the ensemble of conformations describing the heptasaccharide repeating unit. The data in Table 2 indicate that, for the glycosidic linkage between sugars a–b, two main conformations can be considered. These conformations are identified as A1 and A2 and are characterized by their $\phi_{H ab}/\psi_{H ab}$ dihedral angles as A1, $-70/-60$, and A2, $25/-60$. For linkage b–c, four conformers can be proposed: B1, $-75/-55$; B2, $-75/-40$; B3, $15/-55$; and B4, $15/-40$. For linkage g–b, torsion $\psi_{H gb}$ has multiple solutions in the interval $(-35, 55)$ so the conformers are G1, $70/(-35, 55)$, and G2, $30/(-35, 55)$. For the c–d linkage, the main conformers are C1, $-70/(-180, -100)U(80, 180)$, and C2, $120/(-180, -100)U-$

Table 3: Lowest Energy Families Obtained in r-SA and Statistical Weights (p_i) Obtained from SVD Fitting of the Conformational Families to the Scalar Coupling Data for Five Possible Solutions

family	relative energy (kcal mol ⁻¹)	soln 1 (p_i)	soln 2 (p_i)	soln 3 (p_i)	soln 4 (p_i)	soln 5 (p_i)
A1B1G1C1D2E1	0.5	0.44	0.36	0.45	0.39	0.34
A1B3G1C2D1E1	1.3	0.25	0.21	0.25	0.19	0.20
A1B1G1C2D2E1	2.7	0.16	0.24	0.04	0.10	0.20
A1B3G2C1D2E1	1.3	0.05	0.09	0.04	0.10	
A1B4G2C2D2E1	0.8	0.05		0.05		
A1B2G1C2D1E1	4.4	0.04		0.05	0.04	
A1B2G1C1D1E1	3.1	0.01	0.05			0.05
A1B4G1C2D2E1	0.0		0.04		0.05	
A1B4G2C2D1E1	2.1		0.01			
A1B1G1C2D1E1	4.6			0.10	0.11	0.06
A1B3G2C1D1E1	2.3			0.01		0.06
A1B3G1C1D2E1	1.9				0.01	
A1B4G1C1D1E1	5.1					0.05
A1B3G2C2D1E1	4.6					0.04
A1B4G1C2D1E1	3.6					
A1B1G2C1D1E1	4.4					
A1B4G2C1D1E1	1.5					
A1B4G1C1D2E1	3.6					
A1B2G1C1D2E1	5.9					
A1B4G2C1D2E1	2.3					

(80,180).² For the d–e linkage, the possibilities are D1, 70/(-180,-70)U(80,180), and D2, -40/(-180,-70)U(80,180). For the e–f linkage, the conformers are E1, (-20,70)/-60, and E2, (-20,70)/-40. The conformations deduced for each glycosidic linkage of the J22 polysaccharide were then combined to build a complete structure of the heptasaccharide. A total of 64 conformation families A1B1G1C1D1E1, A2B1G1C1D1E1, ..., can be produced by combining the different possibilities. These 64 starting structures were built by setting the angles to the proper values. After restrained minimization, each starting conformation then was submitted to an r-SA protocol as described in the Materials and Methods. Restrictions corresponding to the starting conformation were applied to the glycosidic dihedral angles while the rest of the structure was optimized.

The analysis of the r-SA trajectories showed that only 20 of the 64 different families provided conformers in a low-energy range up to 6 kcal mol⁻¹ over the global minimum. These 20 families, shown in Table 3, are in principle the most satisfactory conformers that can explain the experimental data. Since the glycosidic dihedral angles within the conformers of each family remained close to the imposed constraints, the conformers of each of these 20 families can only explain partially the experimental couplings.

Singular value decomposition (SVD) (34) was used to find linear combinations of the 20 heptasaccharide conformations in which populations of individual dihedral angles correspond to those of Table 2. Since those populations are derived from experimental coupling constants and energetic calculations (SA), this fitting procedure, a mathematical explanation of which is given in the Supporting Information, will yield populations of heptasaccharide conformations which are both energetically reasonable and whose scalar coupling constants agree with experiment. Several solutions are possible depending of the initial trial values used for SVD and five of

these solutions are shown in Table 3. For these and other solutions found, there are always three main families that account for ~0.8 of the total population, which are A1B1G1C1D2E1 (p_i 0.341–0.438), A1B3G1C2D1E1 (p_i 0.193–0.25), and A1B1G1C2D2E1 (p_i 0.045–0.242). The remaining 17 families account for ~0.2 of the population. For any of these remaining families, the population is rather small or even zero depending on the solution.

Experimental Data and Conformation of the Polysaccharide of S. mitis J22. Given the model of Table 3, we can ask whether it can adequately explain the available experimental data. We find that the NOE data are not very sensitive to details of the model but that some minor adjustments are required to make the model fit certain of the vicinal coupling data. Finally, we discuss how the puckering of the galactofuranoside residue model can be adjusted to improve the agreement with some additional data.

A first attempt was made to calculate coupling constants using eqs 2–4 and the populations deduced in solution 1 of Table 3 along with conformations corresponding to the global energy minima of each family. This calculation showed that although the agreement obtained for most of the coupling constants is good, the degree of agreement for the couplings of $\psi_{O_{cd}}$ and $\psi_{O_{de}}$ is poor (data not shown). This observation is related to the fact that for these torsions the coupling constants do not offer enough information to deduce simultaneously angles and statistical weights (see Table 2) so that the restraints applied in r-SA were too loose. But whenever the statistical weight is fixed, then it is possible to deduce information on these angles. To improve the agreement of the model with experimental data, the statistical weights were fixed to the values of the three major conformers of model 1 in Table 3, and then the corresponding theoretical angles of $\psi_{O_{cd}}$ and $\psi_{O_{de}}$ in agreement with C–C and C–H coupling constants were calculated by two independent grid searches using eq 4. Both possibilities for assignment of H6proR and H6proS were considered for residues d and e to reconcile the C–H vicinal coupling constant for $\psi_{O_{cd}}$ with a qualitative analysis of the inter-residue NOEs H1c/H6d,6d', and the vicinal coupling for $\psi_{O_{de}}$ with NOEs H1d/H6e,6e'. In both cases, the C1–O1–C6–H6 coupling constant reported in Table 1 corresponds to the strongest H1–H6 NOE intensity in HMQC–NOESY. This experimental information was incorporated in each grid search by selecting only those solutions that gave the shorter average distance for that H6 proton involved in the vicinal C–H coupling reported. It is remarkable that for both linkages only one of the two possible assignments of H6proR or H6proS is consistent simultaneously with C–C, C–H coupling and this qualitative analysis of NOE data, while no solutions are obtained for the other possibility. The results for the hydroxymethyl group of residue d are consistent only with the assignment of H6dproS to δ 3.736 ppm and H6dproR to δ 4.046 ppm. For the hydroxymethyl group of residue e, H6eproR is assigned to δ 3.732 ppm and H6eproS to δ 3.898 ppm. The solutions obtained in the grid searches allowed further restriction of the intervals of angles of $\psi_{O_{cd}}$ and $\psi_{O_{de}}$ beyond those indicated in Table 2. The new intervals, $\psi_{O_{cd}}$ (-180, -160)U(80, 180) and $\psi_{O_{de}}$ (155,180)U(-70,-90), were used in the final extended r-SA for each of the three most populated conformers.

² The symbol U represents the union of two intervals for a dihedral angle.

Table 4: Glycosidic Dihedral Angles and Statistical Weights for Conformers of the Polysaccharide from *S. mitis* J22 for the Three Main Conformers of Solution 1^a

family	P_i	$\phi_{H ab}$	$\psi_{H ab}$	$\phi_{H bc}$	$\psi_{H bc}$	$\phi_{H gb}$	$\psi_{H gb}$	$\phi_{H cd}$	$\psi_{O cd}$	$\phi_{H de}$	$\psi_{O de}$	$\phi_{H ef}$	$\psi_{H ef}$
A1B1G1C1D2E1 ^b	0.44	-63.6	-58.5	-85.1	-54.6	69.5	40.6	-45.1	-159.2	68.5	158.5	48.9	-55.6
A1B3G1C2D1E1 ^c	0.25	-63.4	-58.4	6.4	-55.1	69.4	35.5	107.3	91.0	-40.9	-147.3	51.3	-54.8
A1B1G1C2D2E1 ^d	0.16	-63.4	-58.2	-84.2	-54.3	69.6	40.4	113.7	124.6	69.9	-69.8	28.9	-56.6
conversion to IUPAC ϕ_o/ψ_o		+120	+120	+120	+120	-120	+120	-120	0	-120	0	-120	-120

^a These conformers are the lowest energy minima obtained in r-SA. A linear combination of these conformers is in agreement with the experimental data (see Table 1). An indication for the conversion of these angles to the IUPAC definition (ϕ_o/ψ_o) is also given. ^b ω_c 59.6, ω_d -65.4, γ_d -176.3, P_d -57.9. ^c ω_c -88.0, ω_d -67.9, γ_d 57.5, P_d -55.8. ^d ω_c -64.5, ω_d 87.1, γ_d -58.9, P_d -57.9.

Table 5: Experimental and Calculated Data for the Galf Ring d Conformation in the Polysaccharide of *S. mitis* J22 for the Three Main Conformers of Solution 1

conformer	pop.	conf. ring d	angle C ₁ O ₄ C ₄ C ₅	³ J _{C1C5} ^a	ⁿ J _{C1C3} path. 1 ^b	angle C ₁ O ₄ C ₄ C ₃	ⁿ J _{C1C3} path. 2 ^c	dist. H1-H2 (Å)	dist. H1-H3 (Å)	dist. H1-H5 (Å)
A1B1G1C1D2E1	0.44	¹ E	-136.0	1.9	-0.22	-11.1	3.5	2.7	4.1	4.6
A1B3G1C2D1E1	0.25	¹ E	-144.2	2.4	-0.13	-18.4	3.3	2.7	4.1	5.2
A1B1G1C2D2E1	0.16	¹ E	-143.0	2.4	-0.13	-18.2	3.3	2.7	4.1	5.2
exptl		north ^d		1.8 ^e			3.4 ^e	0.0147 ^f	0.0057 ^f	0.0017 ^f

^a Calculated for ³J_{C1O4C4C5} using eq 3. ^b Projection sum resultant for ³J_{C1C2C3} (pathway 1). ^c Calculated ³J_{C1O4C4C3} (pathway 2) using eq 3. ^d Deduced by comparison of ¹J_{C1H1} and ¹J_{C2H2} with α -mannose (see text). ^e Experimental value taken from ref 26. ^f NOE normalized intensities taken from ref 23.

Additional information can be introduced to assist in establishing the conformation of the Galf ring d in the polysaccharide from *S. mitis* J22. Serianni and co-workers have pointed out that the ¹J_{CH} values in aldofuranosyl rings depend on C-H bond lengths (42 and references therein), with shorter bonds yielding larger couplings. C-H bond lengths vary with bond orientation with a systematic trend toward shorter lengths when the bond orientation is quasiequatorial and longer bonds when quasi-axial (42). Comparison of the experimental ¹J_{CH} of the J22 polysaccharide with those of analogous compounds of fixed conformation provides some information on the conformation of the Galf ring. The two candidates chosen for this comparison are α -mannoside and β -allose, where the relative disposition of electronegative substituents at C1 and C2 axial-axial and equatorial-equatorial is similar to those of North and South conformers of ring d, respectively. Experimental values of ¹J_{C1-H1} and ¹J_{C2-H2} for residue d in the J22 polysaccharide are 175.5 and 149.6, respectively. For α -mannose, the values reported (43) are 174.3 and 149.5, while for β -allose, the values reported (43) are 163.4 and 143.8. These coupling constants indicate that Galf ring d adopts a North conformation where C1-H1 and C2-H2 bonds are quasiequatorial as in α -mannoside. This analysis of the Galf conformation can be completed by the experimental long-range C-C coupling constants within this ring. The coupling constant ³J_{C1-O4-C4-C5} reported for residue d (26) is 1.8 Hz with the corresponding dihedral angle calculated using eq 3: $-134 \pm 10^\circ$. The experimental ⁿJ_{C1-C3} reported for ring d (26) is 3.4 Hz. Two possible pathways across ring d exist for this coupling constant, which are ²J_{C1-C2-C3} and ³J_{C1-O4-C4-C3}. The contribution of the first pathway can be estimated theoretically by using the projection sum method (38), while the contribution of the second pathway can be calculated using eq 3. A final source of information can be obtained by a qualitative analysis of NOE data within the Galf ring d protons. The normalized intensity (23) of H1-H2 is 0.0147, of H1-H3 is 0.0057, and of H5-H1 is 0.0017. These data suggest that at least H1-H2 distance should be shorter than that of H1-H3 or H5-H1.

The above information concerning the Galf conformation and the restricted intervals deduced for $\psi_{O cd}$ and $\psi_{O de}$ were incorporated in three final r-SA calculations which were designed to find the conformations of the three principal conformers which give the best overall agreement of the model with all the experimental data available. Therefore, North conformations were selected for the Galf residue and a NOE restraint was introduced to hold Galf H1-H2 distance (2.5-3.7 Å) to retain this puckering. The r-SA calculation also included NOE distance restraints. The glycosidic dihedral angles were restrained to the intervals previously used for each of the three principal families with the exception of $\psi_{O cd}$ and $\psi_{O de}$ for which the intervals (-180, -160)U(80, 180) and (155,180)U(-70,-90) were used, respectively. The length of each of the final r-SA simulations was 2 ns with the rest of the conditions as described in the Materials and Methods.

From each of these r-SA, simulations of the three major populated families the lowest energy conformation in agreement with coupling and NOE data for Galf was selected. Table 5 shows the experimental and calculated data concerning the Galf ring for these conformers. While all three conformers adopt ¹E conformation, some local minimum energy conformers adopt ¹T₂ conformations. These puckerings are localized in a single narrow region of the northwest region of the pseudorotation cycle so that a minimum conformational change is required for interconversion ¹E and ¹T₂. Both possibilities are in agreement with the ¹J_{CH} coupling constants. It can be seen in Table 5 that there is also excellent agreement between the experimental and calculated ³J_{C1C5}. The experimental ⁿJ_{C1C3} is in good agreement with the calculated value for pathway 2, and the expected contribution of pathway 1 to this coupling (projection sum method) is very small and slightly negative. Finally, the qualitative analysis of intraresidue NOE distances is also in agreement with the experimental data for these ¹E and ¹T₂ Galf conformations. The possibility of finding other Galf ring conformations different from ¹E or ¹T₂ in agreement with all the experimental data was tested by simulating the

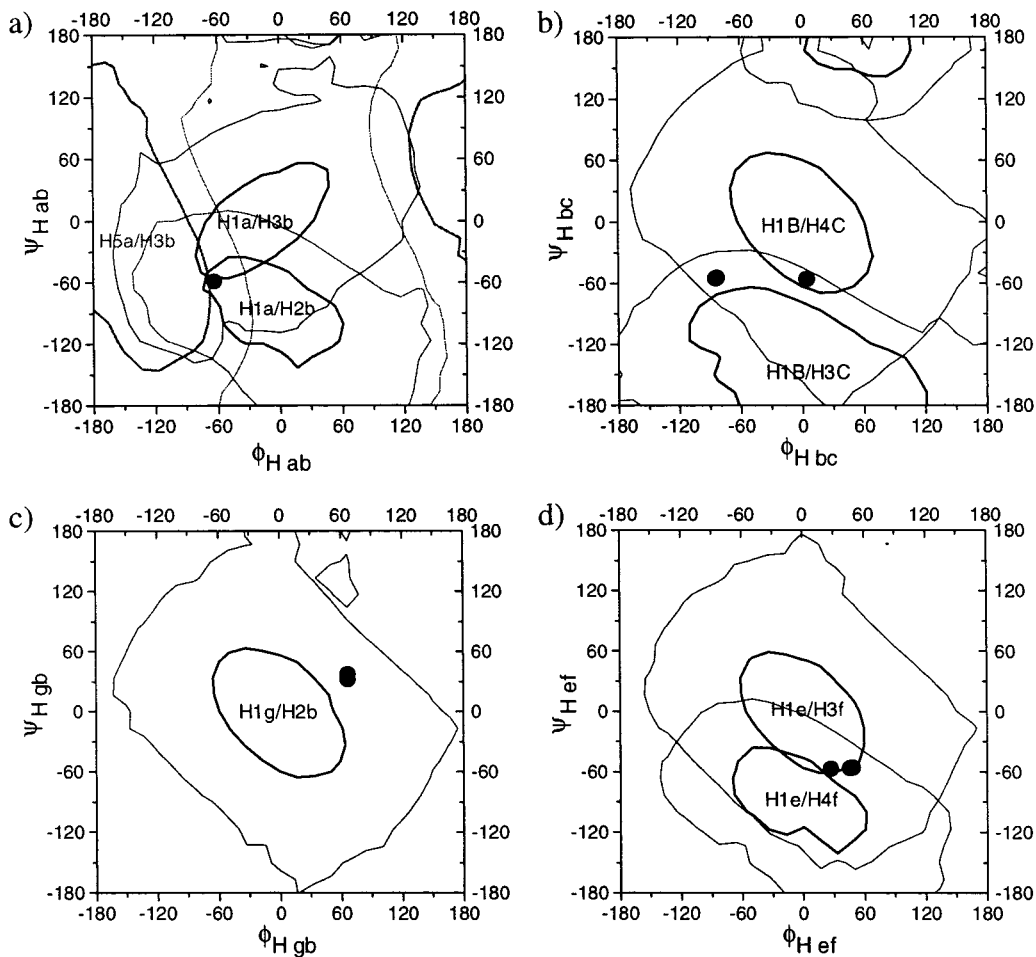


FIGURE 3: NOE distance contours over $\phi_{\text{H}}/\psi_{\text{H}}$ map for different linkages of the polysaccharide from *S. mitis* J22. The contours represented correspond to the strongest interresidue NOE observed. Contours represented in bold line are 2.5 Å and those in normal line 3.5 Å. The black point represents the dihedral angles of the three main conformations of solution 1.

theoretical coupling constants of nine different envelope or twist conformations of Gal_f in the north region of the pseudorotational cycle. These results suggest that the conformation of the Gal_f residue in the *S. mitis* J22 polysaccharide is quite rigid.

A qualitative analysis of the NOE data available for polysaccharide J22 was performed in preference to a more quantitative treatment using a full relaxation approach because of the uncertainties of the time scale for the exchange between conformers and because the assumption of rigid isotropic tumbling may not be justified for this flexible polysaccharide. NOE distance contours of the strongest experimental interresidue NOEs were generated as described in the Materials and Methods (see Figure 3). These contour maps can be used to test whether the three most populated conformers are compatible or not with the strongest experimental NOEs using a two spin approximation.

For residues a–b, the three main conformers present similar values of $\phi_{\text{H ab}}/\psi_{\text{H ab}}$ around $-60/-60^\circ$ which correspond to the common zone of all the NOEs in Figure 3a. For residues b–c, two possible conformations are described by $\phi_{\text{H bc}}/\psi_{\text{H bc}}$ angles around $-85/-55^\circ$ and $5/-55^\circ$, which also corresponds to the common zone of all the NOEs in Figure 3b. For residues g–b, only one conformation is expected around $\phi_{\text{H gb}}/\psi_{\text{H gb}}$ $70/40^\circ$ which, is in agreement with the distance contours of Figure 3c. Finally, for residues e–f, two slightly different conformations

around $\phi_{\text{H ef}}/\psi_{\text{H ef}}$ $50/-55^\circ$ and $\phi_{\text{H ef}}/\psi_{\text{H ef}}$ $30/-55^\circ$ are obtained, which are also in the common zone of all the NOEs of Figure 3d. These observations indicate that the three main conformers obtained are in qualitative agreement with these experimental interresidual NOE data. A calculation of $\langle r^{-6} \rangle$ or $\langle r^{-3} \rangle$ average distances of these $(i, i+1)$ NOE connectivities was performed with these models, and a good agreement is found with the corresponding experimental NOE (23) (Table S1 of Supporting Information). Also the calculation of the average distances between H1c–H6dproR and H1c–H6dproS, as well as the average distances between H1d–H6proR and H1c–H6proS (Table S1 of Supporting Information), are also in qualitative agreement with the experimental NOE intensities and agrees with this stereospecific assignment.

The general shape of the three conformers selected from these three final r-SA (Figure 4) shows that they adopt a loop conformation in the zone of the 1 → 6 linkages (residues c, d, and e). This loop conformation has been previously observed in a molecular modeling study of polysaccharide *S. mitis* J22 (44). The conformations obtained here indicate that the formation of the loop is favored mainly by some favorable van der Waals interactions between the hydrophobic face of rings c, d, e, and f.

It can be seen in Figure 4d that the loop shape adopted for these three main conformers differs substantially among them. Furthermore, in each of the three corresponding r-SA

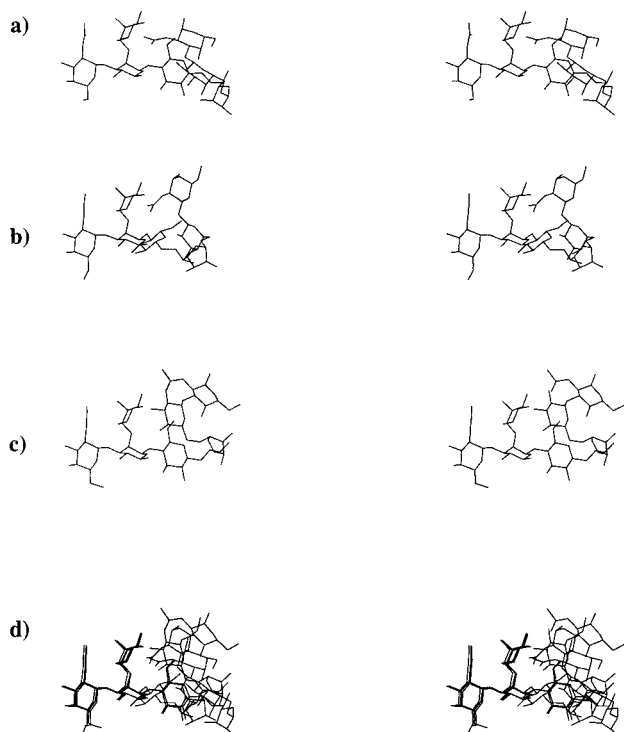


FIGURE 4: Stereoview of the three most highly populated conformations of *S. mitis* J22. (a) family A1B1G1C1D2E1, $p_i = 0.438$. (b) family A1B3G1C2D1E1, $p_i = 0.250$, and (c) family A1B1G1C2-D2E1, $p_i = 0.159$. (d) Superposition of these three conformers with residues a, b, and g aligned.

simulations for these three conformers, there are other minima within a low-energy range that also can explain the experimental data and which have more extended conformations. Since the glycosidic torsions were restricted in these simulations in order to satisfy the coupling and NOE data, the folded and extended conformers are generated by concerted transitions around the ω_c , ω_d , and γ torsions, all at a rather modest energetic cost. Thus, the GalF residue d acts as a kind of hinge, not as a result of furanoside puckering but rather of rotation at its C5–C6 and C4–C5 bonds and at the C5–C6 bond of residue e. The transient nature of the looped conformers illustrated in Figure 4 makes it unlikely that long-range NOE connectivities of the type $(i, i+n)$ for $n > 1$, between protons close in the space but separated for more than one residue in the chain, can be experimentally observed. On the other hand, NOE between residues which are connected by relatively restricted glycosidic torsions can have short average distances during the whole r-SA simulation.

The conformation adopted by the pyranose rings a, b, and g is quite similar in the three main conformers (Table 4 and Figure 4d). These residues have been associated to the antigenic-binding site of this cell wall polysaccharide (45). Relaxation measurements have shown that these are the most rigid residues of the polysaccharide (15). While the glycosidic torsion angles involving residues c, d, and e are defined by quite different dihedral angles, those of linkage e–f show an intermediate degree of flexibility mainly around $\phi_{H\text{ef}}$ (Table 4) also in agreement with the relaxation data (15).

DISCUSSION

In this paper, a study of the conformation of the polysaccharide derived from *S. mitis* J22 has been performed which

extends previous modeling by Xu and Bush (23, 27). This treatment, which includes more experimental data in an effort to reduce ambiguities in the flexible model, reaches the same general conclusions as the previous model with only modest changes required to fit the new data. An ensemble of three main conformations has been deduced, which are in agreement with the available $^3J_{\text{COCH}}$, $^3J_{\text{COCC}}$, and $^2J_{\text{COC}}$ across the glycosidic linkages as well as interresidue NOE data. While the J22 polysaccharide is a comparatively flexible one, its properties can be described by a very few conformations for which the linkages between several of the residues, namely a, b, and g are nearly rigid. Most of the flexibility arises from limited conformational changes of the phospho diester linkages and the 1 \rightarrow 6 linkages connecting residues c, d, and e, which appear to adopt a dynamic equilibrium between a loop type structure and an extended conformation. The structure across the e–f glycosidic linkage is described by a single conformation. The puckering of the GalF ring d is limited to the northwest part of the pseudorotational cycle, adopting exclusively an 1E or 1T_2 conformations.

A new conformational analysis methodology has been proposed which is applicable to cases of flexible polysaccharides such as that from the cell wall of *S. mitis* J22. The strength of this new scheme for flexible polysaccharides comes from its reliance on scalar coupling data. Averages over an ensemble of conformers are much more simple than for the case of NOE data. A second strength comes from the fact that each scalar coupling value can be associated with the glycosidic dihedral angle of a single linkage, effectively uncoupling the degrees of freedom in the initial stages of the model building and greatly simplifying the combinatorial problem inherent in modeling a flexible polymer. Longer range interactions need be incorporated only at later stages of the refinement of the model.

A major problem in model building based on scalar coupling data is introduced by the multiple valued nature of the trigonometric Karplus type correlation curves for which no single value of a dihedral angle can be uniquely associated with a given J value. This study shows that the ambiguity can be resolved with multiple coupling data correlated with each angle. The use of both $^3J_{\text{COCH}}$ and $^3J_{\text{COCC}}$ data in combination with molecular modeling energy calculations was crucial for these cases. This requirement for extensive carbon coupling data raises another issue since long-range scalar coupling data are most conveniently measured in highly ^{13}C enriched samples. Although there are few examples of complex oligosaccharides and polysaccharides with high enrichment, rapid progress in biosynthetic incorporation, in chemical synthesis and in enzymatic synthesis with glycosyltransferases should provide a growing library of samples suitable for studies of this kind.

SUPPORTING INFORMATION AVAILABLE

Procedure for singular value decomposition, one table giving interresidue proton–proton distances (\AA) for the main three conformers and average distances calculated as $\langle r^{-6} \rangle^{-1/6}$ and $\langle r^{-3} \rangle^{-1/3}$ for the ensemble of conformers plus corresponding experimental NOE normalized intensity obtained for polysaccharide *S. mitis* J22 from ref 23, and two figures showing plots of the different glycosidic torsions and the different hydroxymethyl ω torsions of heptasaccharide J22

as a function of energy (kcal mol⁻¹) for the 56 lowest energy conformations obtained during SA, plus the γ torsion and puckering parameter P of the Gal ring d of J22 as a function of energy in these 56 minima. This material is available free of charge via the Internet at <http://pubs.acs.org>.

REFERENCES

1. Bush, C. A., Martin-Pastor, M., and Imberty, A. (1999) *Annu. Rev. Biophys. Biomol. Struct.* (in press).
2. Homans, S. W. (1993) *Glycobiology* 3, 551–55.
3. Rice, K. G., Wu, P., Brand, L., and Lee, Y. C. (1993) *Curr. Opin. Struct. Biol.* 3, 669–74.
4. Lemieux, R. U., Bock, K., Delbaere, T. J., Koto, S., and Rao, V. S. (1980) *Can. J. Chem.* 58, 631–53.
5. Cagas, P., and Bush, C. A. (1990) *Biopolymers* 30, 1123–38.
6. Mukhopadhyay, C., and Bush, C. A. (1991) *Biopolymers* 31, 1737–46.
7. Miller, K. E., Mukhopadhyay, C., Cagas, P., and Bush, C. A. (1992) *Biochemistry* 31, 6703–9.
8. Kogelberg, H., and Rutherford, T. J. (1994) *Glycobiology* 4, 49–57.
9. Duus, J. O., Nifant'ev, N., Shashkov, A. S., Khatuntseva, E. A., and Bock, K. (1996) *Carbohydr. Res.* 288, 25–44.
10. Hricovini, M., Shah, R. N., and Carver, J. P. (1992) *Biochemistry* 31, 10018–23.
11. Rutherford, T. J., Partridge, J., Weller, C. T., and Homans, S. W. (1993) *Biochemistry* 32, 12715–24.
12. Rutherford, T. J., Spackman, D. G., Simpson, P. J., and Homans, S. W. (1994) *Glycobiology* 4, 59–68.
13. Cumming, D. A., and Carver, J. P. (1987) *Biochemistry* 26, 6664–76.
14. Engelsen, S. B., Herve du Penhoat, C., and Perez, S. (1995) *J. Phys. Chem.* 99, 13334–51.
15. Xu, Q., and Bush, C. A. (1996) *Biochemistry* 35, 14512–20.
16. Bonvin, A. J., and Brunger, A. T., (1996) *J. Biomol. NMR* 7, 72–6.
17. Serianni, A. S. (1992) in *Nuclear magnetic resonance approaches to oligosaccharide structure elucidation* Glycoconjugates (Allen, H., and Kisalius, E. C., Ed.) pp 71–102, Marcel Dekker, NY.
18. Gitti, R., Long, G. X., and Bush, C. A. (1994) *Biopolymers* 34, 1327–38.
19. Milton, M. J., Harris, M. A., Probert, M. A., Field, R. A., and Homans, S. W. (1998) *Glycobiology* 8, 147–53.
20. Bose, B., Zhao, S., Stenutz, R., Cloran, F., Bondo, F., Bondo, G., Hertz, B., Carmichael, I., and Serianni, A. (1998) *J. Am. Chem. Soc.* 120, 11158–73.
21. Church, T., Carmichael, I., and Serianni, A. S. (1996) *Carbohydr. Res.* 280, 177–86.
22. Tvaroska, I., and Taravel, F. (1995) *Adv. Carbohydr. Chem. Biochem.* 51, 15–61.
23. Xu, Q., and Bush, C. A. (1996) *Biochemistry*, 35, 14521–9.
24. van Gunsteren, W. F., Brunne, R. M., Gros, P., van Schaik, R. C., Schiffer, C. A., and Torda, A. E. (1994) *Methods Enzymol.* 239, 619–54.
25. Cuniassse, P., Raynal, I., Yiotakis, A., and Dive, V. (1997) *J. Am. Chem. Soc.* 119, 5239–48.
26. Xu, Q., Bush, and C. A. (1998) *Carbohydr. Res.* 306, 335–9.
27. Xu, Q., Mohan, S., and Bush, C. A. (1996) *Biopolymers* 38, 339–53.
28. Fesik, S. W., and Zuiderweg E. R. P. (1988) *J. Magn. Reson.* 78, 588–93.
29. Abeygunawardana, C., Bush, C. A., and Cisar, J. O. (1990) *Biochemistry* 29, 234–48.
30. Saenger, W. (1983) in *Principles of Nucleic Acid Structure*, Springer-Verlag, Berlin.
31. Nilges, M., Clore, G. M., and Gronenborn, A. M. (1988) *FEBS Lett.* 239, 129–36.
32. Hagler, A. T., Lifson, S., and Dauber, P. (1979) *J. Am. Chem. Soc.* 101, 5122–30.
33. Microcal Origin v.3.5, Microcal Software, Inc.
34. Press, W. H., Teukolsky, S. A., Vetterling, W. T., and Flannery, B. R. (1992) in *Numerical Recipes in C*, pp 59–70, Cambridge University Press, Cambridge, U.K.
35. Mathcad v5.0, MathSoft inc.
36. Tvaroska, I., Hricovini, H., and Perakova, E. (1989) *Carbohydr. Res.* 189, 359–62.
37. Serianni, A., Bondo, P. B., and Zajicek, J. (1996) *J. Magn. Reson., Ser. B* 112, 69–74.
38. Zhao, S., Bondo, G., Zajicek, J., and Serianni, A. S. (1998) *Carbohydr. Res.* 309, 145–52.
39. Homans, S. W., and Forster, M. (1992) *Glycobiology* 2, 143–51.
40. Naidoo, K. J., and Brady, J. W. (1997) *Chem. Phys.* 224, 263–73.
41. Mukhopadhyay, C. (1998) *Biopolymers* 45, 177–90.
42. Podlasek, C. A., Stripe, W. A., Carmichael, I., Shang, M., Basu, B., and Serianni, A. S. (1996) *J. Am. Chem. Soc.* 118, 1413–25.
43. Serianni, A. S., Wu, J., and Carmichael, I., (1995) *J. Am. Chem. Soc.* 117, 8645–8650.
44. Cassels, F. J., Hughes, C. V., and Nauss, J. L. (1995) *J. Ind. Microbiol.* 15, 176–185.
45. Cisar, J. O., Sandberg, A. L., Reddy, G. P., Abeygunawardana, C., and Bush, C. A. (1997) *Infect. Immun.* 65, 5035–5041.

BI9904205